Consolidation of Metal Oxide Nanocrystals. Reactive Pellets with Controllable Pore Structure That Represent a New Family of Porous, Inorganic Materials

Ryan Richards,[1a] Weifeng Li,[1a] Shawn Decker,[1b] Chet Davidson,[1b] Olga Koper,[1b] Vladimir Zaikovski,[1c] Alexander Volodin,[1c] Thomas Rieker,[1d] and Kenneth J. Klabunde*,[1a,b]

Contribution from the Department of Chemistry, Kansas State University, Manhattan, Kansas 66506, Nantek, Inc., 1500 Hayes Drive, Manhattan, Kansas 66502, Boreskov Institute of Catalysis, Novosibirsk 630090, Russia, and Department of Chemical and Nuclear Engineering, University of New Mexico, Albuquerque, New Mexico 87131

Received December 15, 1999

Abstract: Nanocrystals of MgO (4 nm) exist as polyhedral structures with high surface concentrations of edge/corner sites. In powder form the crystallites weakly agglomerate into porous weblike structures of approximately 1400 nm according to small-angle X-ray scattering. Upon consolidation of these fine powders under pressure, pellets can be readily prepared that maintain their high surface areas, and small crystallite sizes. In addition, large pore volumes and pore size openings can be controllably decreased with pelletization pressure increase. The pellets retain their voracious adsorbent affinities and capacities for a wide variety of organic molecules and acid gases. Quantitative measurements on the adsorption of a series of alcohols vs pelletization pressure reveal a pattern of molecular size selectivity.

Introduction

Oxides of many metals are highly ionic and high melting, and their surfaces exhibit both Lewis base and Lewis acid character.[2] These solid acid/base properties are particularly strong at corner/edge sites.[3] Residual surface hydroxyls and cation/anion vacancies can also add to the rich surface reactivities such oxides exhibit.

These surface characteristics allow many metal oxides, especially MgO, CaO, Al_2O_3, TiO_2, ZnO, and others, to be excellent adsorbents for a wide variety of adsorbates, including polar organics and acid gases. In addition, numerous catalytic processes have been discovered that depend on the solid acid/solid base properties of these materials.[2,4] On the other hand, since these oxides are usually prepared by high-temperature processes, surface areas are generally low, and so their use as adsorbents has not been fully exploited.

In recent years numerous reports on the synthesis of nanocrystalline oxides with high surface areas have appeared.[5−10] Indeed, in our hands, nanocrystalline MgO, CaO, and Al_2O_3 have exhibited voracious adsorbent properties due to both enhanced surface areas and intrinsically higher surface reactivities.[11,12] We have concluded that this inherently higher surface reactivity is due to particle size and shape.

Herein we report additional data about shape for nanocrystalline MgO, characterization of aggregates of these nanocrystals, and the properties of pressure formed pellets. These data suggest that nanocrystalline MgO as well as other oxides could make up a broad new family of porous, inorganic adsorbents and catalysts, reminiscent of zeolites and high surface area silica (e.g. MCM-41), but with the added advantages of mechanical pore volume/size control and chemical control of acid/base properties.

Results and Discussion

A. Nanocrystalline Powders: Synthesis, TEM, and SAXS Data. In this work two types of nanocrystalline oxides were prepared; a "conventional preparation" (CP), and an "aerogel preparation" (AP).[3c,9,11,12] Nanocrystalline MgO was prepared by a modified aerogel procedure, yielding a fine, white powder of 400−500 m^2/g and 4 nm average crystallite size. High-resolution TEM imaging of a single crystallite indicated a polyhedral structure suggesting the presence of high surface concentrations of edge/corner sites, and various exposed crystal planes (such as 002, 001, 111).[3b]

(1) (a) Kansas State University. (b) Nantek, Inc. (c) Boreskov Institute of Catalysis. (d) University of New Mexico.

(2) Tanabe, K. *Solid Acids and Bases*; Academic Press: New York, 1970.

(3) (a) Knozinger, H.; Ratnasamy, P. *Catal. Rev. Sci. Eng.* **1978**, *17*, 31. (b) Knozinger, E.; Jakob, K. H.; Singh, S.; Hoffman, P. *Surf. Sci.* **1993**, *290*, 288. (c) Koper, O.; Lagadic, I.; Volodin, A.; Klabunde, K. J. *Chem. Mater.* **1997**, *11*, 2468−2480.

(4) Nieves, I.; Klabunde, K. J. *Mater. Chem. Phys.* **1988**, *18*, 485−498.

(5) Livage, J.; Sanchez, C.; Babonneau, F. Molcular Precursor Routes to Inorganic Solids. In *Chemistry of Advanced Materials*; Interrante, I. V., Hampden-Smith, M. J., Eds.; Wiley-VCH Publishers: New York, 1998; p 389.

(6) Gesser, H. D.; Goswami, P. C. *Chem. Rev.* **1989**, *89*, 765.

(7) (a) Teichner, S. J. *4th International Congress on Catalysis*; Taniguchi Foundation, Kobe, Japan, October 1985; p 59. (b) Teichner, S. J.; Nicolaon, G. A.; Vicarini, M. A.; Gardes, G. E. E. *Adv. Colloid Interface Sci.* **1976**, *5*, 245.

(8) Hench, L. L.; West, J. K. *Chem. Rev.* **1990**, *90*, 33.

(9) Utamapanya, S.; Klabunde, K. J.; Schlup, J. R. *Chem. Mater.* **1991**, *3*, 175−181.

(10) Stark, J. V.; Park, D. G.; Lagadic, I.; Klabunde, K. J. *Chem. Mater.* **1996**, *8*, 1904−1912.

(11) Khaleel, A.; Kapoor, P. N.; Klabunde, K. J. *Nanostruct. Mater.* **1999**, *11*, 459−468.

(12) Klabunde, K. J.; Stark, J. V.; Koper, O.; Mohs, C.; Park, O. G.; Decker, S.; Jiang, Y.; Lagadic, I. *J. Phys. Chem.* **1996**, *100*, 12142−12153.

(13) Rieker, T. P.; Misono, S.; Ehrburger, D. *Langmuir* **1999**, *15*, 914.

10.1021/ja994383g CCC: $19.00
Published on Web 05/05/2000

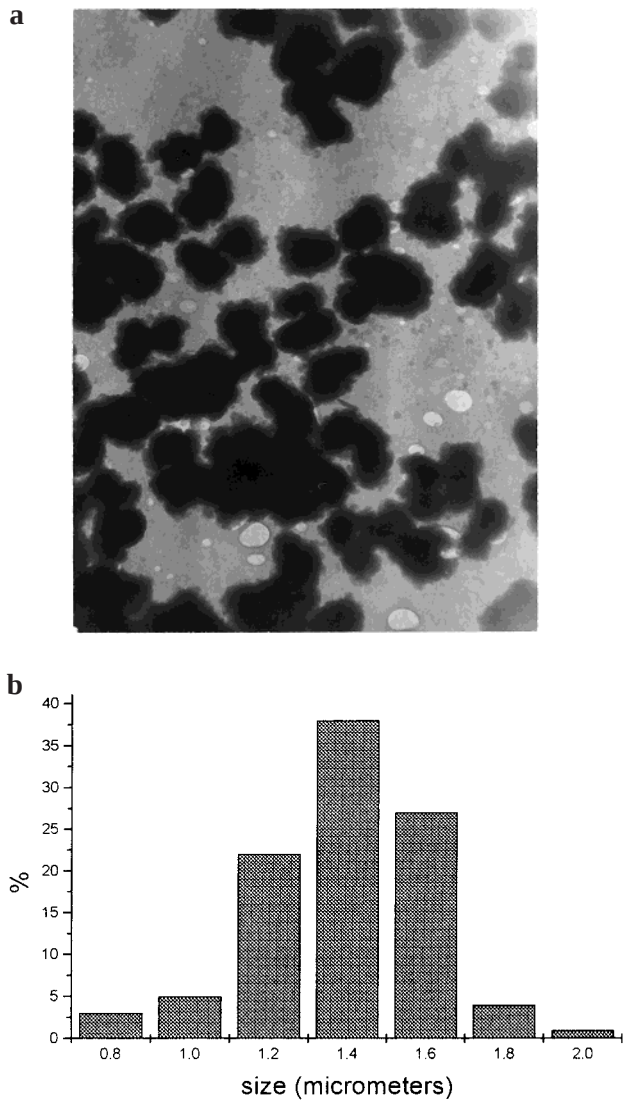

Figure 1. (a) TEM Images of AP-MgO porous aggregates that exist in the as prepared powder. These are formed from interactions of 4 nm crystallites. (b) Bar graphs showing observed size distributions of weblike porous aggregates.

Imaging at lower magnification shows the presence of porous weblike aggregates in the range of about 1400 nm (Figure 1a) that exist in the as prepared powder. These are formed by interaction of the 4 nm (average) crystallites, and their overall size distribution is surprisingly narrow (Figure 1b).

Further investigation of the as prepared powder samples by high-resolution TEM revealed why these porous networks form on the nanoscale. Figure 2 shows a micrograph at essentially atomic resolution, revealing the lattice planes for Mg and O ions. Note the "cubelike" crystallites that aggregate into polyhedral structures with numerous corner/edge sites, and the embryonic formation of pores between those crystalline structures. Plates of the crystalline lattice show a lattice spacing of 2.1 Å corresponding to the (002) planes of MgO. Cubic nanocrystals are shifted along the (001) coalescence faces. This results in the appearance of many steps of subatomic size on the surface of the "cubes" with the egress of the edges and corners of the cubic particles to the external surface. The particle size distribution histogram indicates 10−30 Å cubic crystals and, in this photograph, about 20 Å average size (although powder XRD broadening indicates an average of 40 Å (4 nm)).

To learn more about the microstructure of the powder, small-angle X-ray scattering experiments were carried out. It was necessary to investigate the precursors (hydroxides) as well as the final product (oxides) of both magnesium and calcium systems.

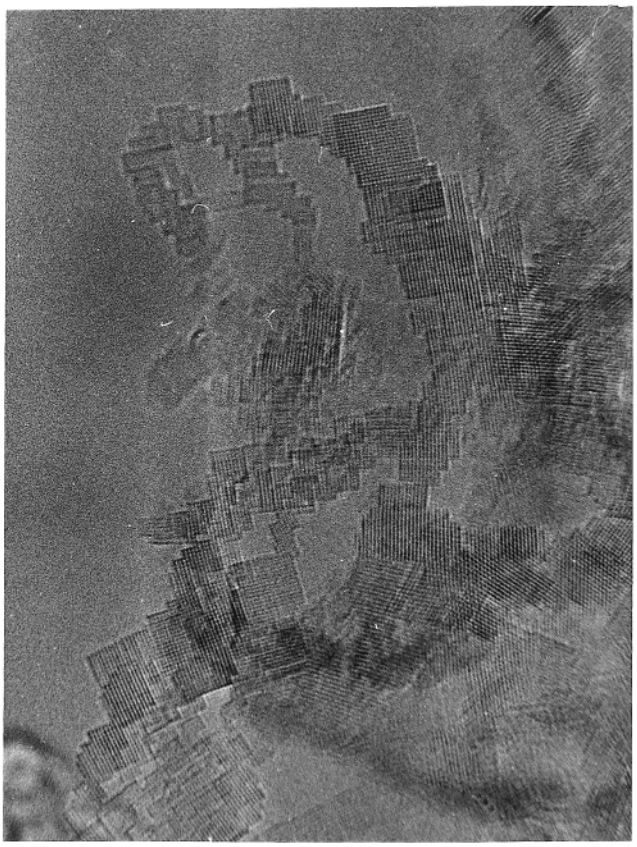

Figure 2. High-resolution TEM of AP-MgO. Note the cubelike nanocrystals that amalgamate into polyhedral structures with many corner/edges, and the embryonic pore structure.

The SAXS data[14−17] for AP-MgO demonstrated a Guinier region (a curved region which nearly flattens out around $q \sim 0.1$ Å $^{-1}$), see Figure 3. Guinier regions arise from characteristic feature sizes within a sample that does not form mass fractal aggregates. For this AP-MgO sample, the high q pore law is -4, which is indicative of a nonfractal surface morphology of the primary particles which the SAXS data indicate are about 100 Å in diameter, and these primary particles aggregate to porous particles of $d \sim 9250$ Å, or about 1 μm. For pelletized (compressed) samples (3000 and 10000 lb force), the Guinier region is not present, and the data indicate that the sample is denser and more isotropic. In other words, the 1 μm aggregates no longer exist, but are pressed together to form a continuous, nonfractal, porous piece.

For the AP-$Mg(OH)_2$, which is the precursor to the AP-MgO, a structure similar to AP-MgO is indicated by SAXS, and the primary particle size is about 92 Å. However, the high q power law slope is -3.3, which is an indicator of a surface fractal morphology unit Ds = 2.7.

For comparison, AP-CaO and AP-$Ca(OH)_2$ samples were also analyzed. For the $Ca(OH)_2$ sample the data suggest a primary

(14) Rieker, T. P.; Hanprasopwattana, A.; Datye, A.; Hubbard, P. *Langmuir* **1999**, *15*, 638.
(15) Sorensen, C.; Oh, C.; Schmidt, P. W.; Rieker, T. P. *Phys. Rev. E* **1998**, *58*, 4666.
(16) Beaucage, G. *J. Appl. Crystallogr.* **1995**, *28*, 717.
(17) *CRC Handbook of Chemistry and Physics*, 75th ed.; CRS, Boca Raton, FL, 1994; pp 4−72.

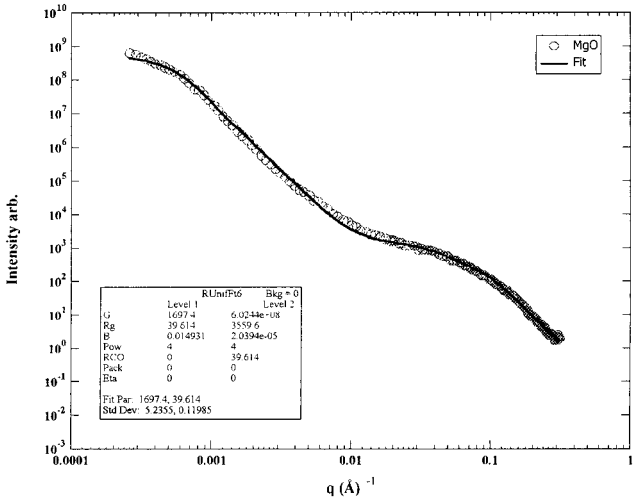

Figure 3. Small-angle X-ray scattering of AP-MgO.

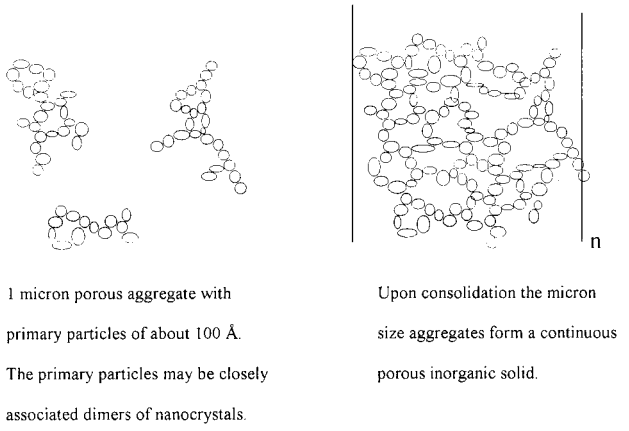

Figure 4. Illustrations of structure of porous aggregates of MgO, as determined by SAXS.

particle size of about 170 Å and that these particles possess a rough surface (surface fractal dimension Ds = 2.0).

In summary, the SAXS data suggest that the hydroxide samples exist as rough primary particles that are possibly made up of 2 or 3 fundamental crystallites, and these exist as 100 nm porous aggregates. Upon conversion to the oxides, those general structural features are retained. In the case of calcium samples, some fractal nature can be ascertained, but in magnesium samples the porous, weblike aggregates are 10 times larger, and are highly porous without a fractal nature. Upon pressing into pellets, the 1 μm aggregates came together into a continuous porous pellet (Figure 4).

B. Nanocrystalline Pellets: Pore Structure and Adsorption Properties. Pelletized samples introduced in the last section will now be described in more detail. Compression of the nanocrystalline powders was carried out by pressure applications at room temperature using a hydraulic press. For example, AP-MgO powder possessed a low density of about 0.30 cm^3/g. Upon compression at low pressure (3000 lb) this increased to 0.58 cm^3/g, and at 6000 lb to 0.63 cm^3/g, and at 20000 to 1.0 cm^3/g (the bulk density of crystalline MgO is 3.58 cm^3/g).[18]

Table 1 summarizes surface areas and other data obtained by BET nitrogen adsorption at 77K for AP-$Mg(OH)_2$, and Table 2 for a series of nanocrystalline oxides. Tables 3 and 4 compare results for MgO prepared by first compressing the hydroxide followed by heat conversion to MgO, with compression of already formed MgO.

First, it is noted that there is little difference in the final pellet whether the $Mg(OH)_2$ precursor is compressed and then heat converted or if already formed MgO is compressed. In both cases surface areas change very little, and pore volumes and pore radii also remain essentially unchanged when low to moderate pressures are used. Only when very high pressures are used are the properties changed, for example, $Mg(OH)_2$ pelletized at 5000 lb shows some pore volume and pore radii shrinkage, and these changes increase as expected at 10000 and then 20000 lb (Table 1). Actually, it appears that these properties can be roughly controlled by the pressure applied.

(18) Lowell, S. *Introduction to Powder Surface Area*; John Wiley & Sons Publishers: New York, 1979; p 63.

Table 1. Surface Area and Pore Size Distribution of Magnesium Hydroxide in Powder and Pellet Forms

sample load (lbs)	surface area (m^2/g)	total pore vol (cm^3/g)	crystallite size (nm)	av pore diameter (Å)
powder	364	0.898	4.7	98.7
1000	371	0.833	4.5	89.7
2000	359	0.660	4.7	73.4
3000	370	0.670	4.2	72.6
5000	366	0.586	4.3	64.1
10000	383	0.436	4.3	45.5
20000	342	0.290	4.3	33.9

Table 2. Summary of Pore Structure and Surface Area of a Series of Oxides

sample description	multi-point surface area (m^2/g)	single-point surface area (m^2/g)	total pore vol (cm^3/g)
CP-MgO pressed after activation			
powder	235	241	0.438
medium compression	255	251	0.287
high compression	241	235	0.311
AP-MgO pressed before activation			
powder	343	334	0.681
low compression	351	340	0.715
medium compression	337	328	0.684
high compression	341	330	0.677
AP-MgO pressed before activation			
powder	343	334	0.681
low compression	335	324	0.676
medium compression	331	321	0.657
high compression	326	316	0.613
CP-CaO pressed before activation			
powder	133	128	0.233
medium compression	93	91	0.154
high compression	80	77	0.144
CP-CaO pressed before activation			
powder	133	128	0.233
medium compression	93	91	0.154
high compression	80	77	0.144
CP-CaO pressed after activation			
powder	133	128	0.233
medium compression	105	102	0.173
high compression	132	130	0.212
AP-CaO pressed before activation			
powder	129	120	0.198
low compression	137	133	0.220
medium compression	144	135	0.231
high compression	135	128	0.222
AP-CaO pressed after activation			
powder	129	120	0.198
low compression	141	137	0.234
medium compression	141	134	0.228
high compression	146	141	0.244

[a] Activation refers to heating under vacuum at 500 °C either before or after pressing. Activated after pressing means that the hydroxide was pressed and upon activation, the hydroxide pellets were converted to the oxide. [b] Medium compression is 1400 lb load and high compression is 1900 lb load.

Table 3. Surface Area and Pore Size Distribution of Magnesium Oxide Prepared by Compression of the Hydroxide Followed by Heat Treatment Conversion to MgO

form	relative compression	surface area (m^2/g) multi-point	surface area (m^2/g) single-point	total pore vol (cm^3/g)	av pore radius (Å)	pore shape type
powder	none	221	334	0.682	61.9	E
pellet	low	222	340	0.715	64.5	A, E
pellet	medium	214	328	0.684	63.9	A, E
pellet	high	214	330	0.677	63.4	A, E

Table 4. Surface Area and Pore Size Distribution of Compressed Magnesium Oxide

form	relative compression	surface are (m^2/g) multi-point	surface are (m^2/g) single-point	total pore vol (cm^2/g)	av pore radius (Å)	pore shape type
powder	none	221	334	0.682	61.9	E
pellet	low	210	324	0.676	64.3	A, E
pellet	medium	205	321	0.657	64.1	A, E
pellet	high	199	316	0.613	61.6	A, E

Another interesting aspect is that the powders exhibit adsorption/desorption isotherms typical of bottleneck pores (type E),[18] in which, after compression at 1000 lb of pressure, all samples of $Mg(OH)_2$ and MgO exhibit bottleneck and cylindrical pores, open at both ends (types A and E).

Table 2 gives data for CP and AP samples of magnesium and calcium oxides and hydroxides. The CP samples were more susceptible to collapse of pore volume, especially the calcium samples. However, the AP-calcium samples exhibited more resistance. Overall, the AP-magnesium samples showed the most resistance to pore volume loss, followed by AP-calcium, then CP-magnesium, and CP-calcium samples showed the least resistance.

A logical conclusion is that the AP-oxides, due to their polyhedral nanocrystal shapes and their tendencies toward forming porous weblike aggregates, are the most resistant to collapse under pressure. The CP-oxides, perhaps due to their more ordered hexagonal platelet shapes,[3c] more easily compress into more dense structures.

One additional feature that is intriguing is that in nearly all experiments carried out with MgO, compressing the powders at low or low-medium pressures led to slightly *higher* surface areas. This remarkable, but reproducible feature is hard to explain, but is reflected again in adsorption properties, as discussed below.

Perhaps it is not surprising that these highly porous pellets are excellent adsorbents for a variety of organic and inorganic adsorbates, and generally mimic the free powders.[11,12,19,20] Herein we describe some of the studies carried out to date, the first one being a gravimetric analysis of CH_3OH adsorption rates for several trials with the free AP-MgO powder compared with pellets. First note the reproducibility of the powder trials. Then note the 1000, 2000, and 5000 lb load pellets that fall in the same range, in fact the 2000 lb samples exhibited the highest adsorption rate, perhaps due to the unexpected surface area increase upon mild compression noted before. However, the most important finding is that as pelletization pressure is increased to 10000 and 20000 lb where significant surface area and pore structure collapse has been demonstrated, the expected lower adsorption rate and lower capacity is realized. This finding correlates nicely with the nitrogen BET pore structure data.

(19) Stark, J. V.; Klabunde, K. J. *Chem Mater.* **1996**, *8*, 1913−1918.
(20) Lucas, E. M.; Klabunde, K. J. *Nanostruct. Mater.* **1999**, *12*, 179−182.

Table 5. Calculated Diameters of Alcohol Molecules

	CH_3OH	CH_3CH_2OH	$CH_3CH_2CH_2CH_2OH$
diameter of free rotating molecule	2.8 Å	4.0 Å	6.5 Å
freely rotating area	7.9 $Å^2$	16.3 $Å^2$	42.9 $Å^2$
pinned at oxygen and sweeping a circular area πr^2	13 $Å^2$	35 $Å^2$	107 $Å^2$

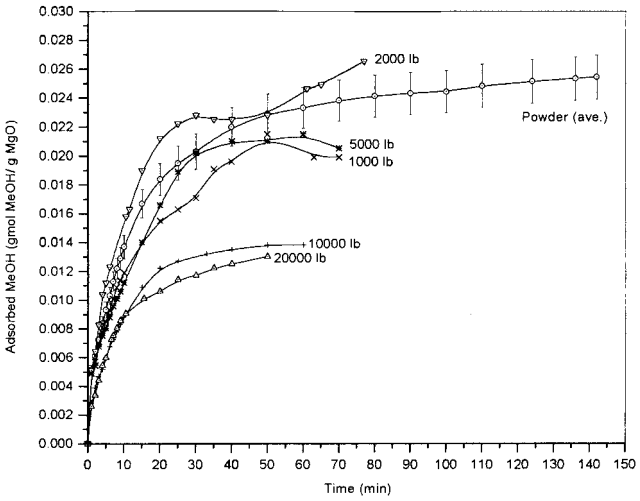

Figure 5. Adsorption of methanol (100 Torr) by AP-MgO compressed to pellets at different loads.

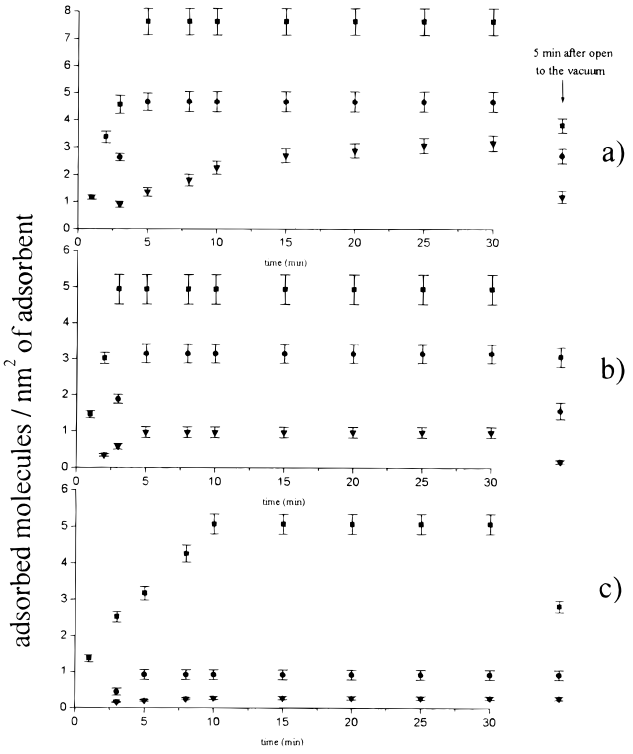

Figure 6. Adsorption of alcohol molecules at 5 Torr (■, methanol, ●, ethanol, ▼, *n*-butanol): (a) uncompressed AP-MgO, (b) AP-MgO compressed with 5000 lb, (c) AP-MgO compressed with 20000 lb.

Next, a study of a series of alcohols of varying sizes was carried out, each at a pressure of 5 Torr of the alcohol. Figure 6 shows rates and amounts adsorbed for CH_3OH, EtOH, and *n*-BuOH. In this study, we were interested in whether adsorption amounts could be controlled by molecular size vs pore size/volume which in turn was controlled by pellet compression load. It is clear from the figure that adsorption can be dramatically

affected by compression load vis-à-vis molecular size. Both Figures 5 and 6 show that the uncompressed powders freely adsorb methanol; indeed at 100 Torr about 15 molecules/nm^2 are adsorbed on the powder, and this drops to about 10 on the high-pressure compressed pellets. These amounts represent over a monolayer, since it can be estimated from molecular size that a monolayer would consist of about 7 CH_3OH/nm^2 of MgO.

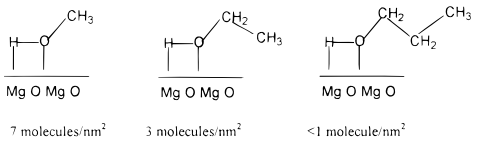

Similarly, if one considers the molecular size of these alcohols, and compares them with the pore sizes/volumes shown for the pellets in Table 4, it seems likely that an important feature is the molecular diameter of the freely rotating molecules. In the case of EtOH and BuOH, the adsorption rate and amount are greatly restricted on the highly compressed samples.

Experimental Section

A. Synthesis of AP- and CP-Metal Oxide Nanocrystals. Detailed synthesis methods for the oxide samples were described in the references cited herein.[3c,9] In short, aerogel prepared (AP-) metal oxide was prepared by sequential methoxidation, hydrolyzation, hypercritical drying, and heat treatment under vacuum. Thus, clean metal pieces were dissolved in methanol under an inert atmosphere to form metal methoxide; upon vigorous stirring for a few hours, deionized water was added dropwise to form a hydroxide gel, which was dehydrated in an autoclave and heated under dynamic vacuum to yield the nanometer-sized metal oxide.

Conventional prepared (CP-) metal oxide was prepared by reacting the ultrapure commercial metal oxide with deionized water under moderate temperature (~120 °C). The resultant metal hydroxide was then heated under dynamic vacuum to remove the water component forming the desired metal oxide.

B. Pelletization (Compression) Procedures. 1. Pellet Press. A hydraulic press (Fred S. Carver Inc., NJ) with the applied loads ranging from 0 to 24000 lb was used to manually compress the oxide powders into pellets.

2. Automatic Pelletizer. A Stokes Tablet Machine (model E from F. J. Stokes Machine Co., PA) was used to make pellets with various compressions from powdered materials. The pressure applied to the powder could be determined by how far the top of the punch travels into the die of the machine. After checking the pressure settings, the machine was turned on and the pellets automatically pressed.

C. Transmission Electron Microscope Studies. A JEOL JEM-2010 electron microscope with the resolution of 1.4 Å was used for obtaining atomic-scale images. Oxide samples were dissipated in toluene, then a drop of the solution was placed on a fine mesh copper grid, solvent evaporated, and observed under desired magnifications.

D. Small Angle X-ray Scattering. Small-angle X-ray scattering measurements were performed at the University of New Mexico/Sandia National Laboratories Small-angle Scattering Laboratory. Samples ~0.03−0.1 mm thick were prepared by spreading the powders on cellophane tape used as windows on a 1.5 cm inner diameter washer. Data were collected for the four samples and tape backgrounds on both the Bonse-Hart and 5 m pinhole (short geometry) instruments. Scattering data from the two instruments are corrected for background, slit smearing, and sample thickness before being combined. Note, the intensity is not on an absolute scale.

SAXS data are plotted as intensity vs q on log−log plots, where q is given by,

$$q = \frac{4\pi}{\lambda}\sin(2\theta/2)$$

where 2θ is the scattering angle. Power laws ($I(q) = CqP$) are readily seen as straight line segments in log−log plots of intensity vs q. The quantity $1/q$ can be thought of as a yardstick. Scattering features at high q correspond to small structures. Conversely, scattering at low q corresponds to large structures.

E. Adsorption Studies. 1. Nitrogen BET Pore Structure Analysis. The specific surface areas and pore size distributions of the oxide samples were measured by a Quantachrome Flowsorb II 2300 instrument (Micromeritics Co., GA), after 15 min of evacuating the particles under N_2 at 140 °C. The nitrogen adsorption isotherms were obtained at 77 K.

2. Alcohols. High-purity alcohols were directly purchased and used (Fisher Scientific, NJ). Initially, the alcohol vapor was introduced into the system and kept at 5 Torr to interact with the metal oxide preloaded on a quartz crystal microbalance. The weight change of the balance was telescopically monitored and converted to the number of alcohol molecules coated on each square nanometer of the oxide surface. After the adsorption continued for 30 min, the system was open to ultrahigh vacuum to evacuate the alcohol molecules that had been physically adsorbed.

Conclusions

Nanocrystals of metal oxides, in particular alkaline earth oxides, are voracious adsorbents, due to unique morphological features and high surface areas. The unique morphological features are manifested in polyhedral nanocrystals (4 nm for MgO) that self-aggregate into porous weblike structures of approximately 1 μm in diameter.

Upon compression of these powders this porous reactive nature is maintained at low-medium loads, but at high loads pore size and volume can be decreased in a controllable way. Adsorption experiments with alcohols illustrate that compression loads do significantly affect and control adsorption alcohols of varying molecular sizes.

In general it can be said that nanocrystalline oxides represent a new family of porous inorganic materials where pore structure can be roughly controlled by compression techniques.

Acknowledgment. Investigations by Thomas Rieker were carried out under the Small Business Initiative program of Sandia Laboratory and the University of New Mexico. Also, we thank Professor Chris Sorensen for aid in SAXS interpretation. Financial support was provided by the Army Research Office, the Center for Indoor Air Research, and the Hazardous Substance Research Center.

JA994383G